CHEMISTRY OF MATERIALS

COMMUNICATION

pubs.acs.org/cm

Shape Transformation of Gold Nanoplates and their Surface Plasmon Characterization: Triangular to Hexagonal Nanoplates

Soonchang Hong,[†] Kevin L. Shuford,*[,§] and Sungho Park*[,†,‡]

[†]Department of Chemistry and [‡]Department of Energy Science and SKKU Advanced Institute of Nanotechnology, Sungkyunkwan University, Suwon 440-746, South Korea

[§]Department of Chemistry, Drexel University, 3141 Chestnut Street, Philadelphia, Pennsylvania 19104, United States

Supporting Information

KEYWORDS: hexagonal nanoplate, gold nanoparticle, surface plasmon resonance, nanoprism, shape transformation

Because the optical properties of metal nanoparticles are known to be dependent primarily on their shape and size, one of the desired structural goals for these materials is to obtain a uniform size and morphology in a controlled fashion.[1−3] Many literature reports describe the preparation routes of various nanostructures, including spherical, rodlike, cubic, and planar nanoparticles.[4−6] However, only a few methods have been developed for preparing nanoparticles with good control over their sizes and homogeneities, with which one can systematically study the optical properties of such nanostructures.[7−9] Among the many different shapes of metal nanoparticles, anisotropic nanoparticles are particularly interesting because the decreased symmetry allows one to tune their optical properties to a great extent. For instance, elongated nanostructures (or nanorods) exhibit two types of localized surface plasmon resonance (SPR) modes − one oscillating along the short axis and the other along the long axis.[10−12] These modes can be fine-tuned by controlling geometric parameters such as diameter and length. Also, plate-like nanostructures like nanodisks allow a similar tunability in their optical properties resulting from in-plane and out-of-plane modes. Another representative example in this context is the triangular prism (also referred to as nanoprisms) and their synthetic route is well-developed.[13] The ratio of surface to bulk atoms of plate-like nanostructures is higher than that of other nanostructures; therefore, it is expected that the SPRs of nanoplates will be very sensitive to the dielectric medium, including binding of adlayer molecules and solvent that surrounds them. The SPR sensitivity to dielectric constant of the medium is important for developing highly efficient chemical and biological sensors based on the SPR shifts. Herein, we present the synthetic route of hexagonal nanoplates and their corresponding optical properties. Our synthetic method relies on the synthesis of triangular nanoplates that is followed by shape transformation under mild reduction conditions, leading to the formation of hexagonal nanoplates.[14] The higher-order multipole SPRs of such structures could be resolved and compared with theoretical results for the first time.

Figure 1 shows a schematic diagram of the steps involved in the synthesis of hexagonal nanoplates. Their corresponding FESEM images are displayed in Figure 2. First, triangular nanoplates were prepared by following the previously reported method. They show fairly homogeneous size (edge L = 136 (±8) nm, thickness = 8 (±1) nm) and shape distribution. In the synthesis, $AuCl_4^-$ ions were reduced by ascorbic acid in the presence of CTAB and small amount of iodide ions. The concentration of I^- played a critical role in determining the shape of resulting nanoparticles, as suggested in the previous publication.[15] At a certain concentration of iodide, the reaction predominantly leads to the formation of triangular nanoplates. Second, $AuCl_4^-$ ions are added to the triangular nanoplate solution in order to etch selectively the tips of triangular nanoplates. The standard redox potential of $AuCl_4^-$ ($AuCl_4^- + 2e^- \rightarrow AuCl_2^- + 2Cl^-$, E^o: 0.926 V) is lower than that of $AuCl_2^-$ ($AuCl_2^- + e^- \rightarrow Au(s) + 2Cl^-$, E^o: 1.154 V).[16] Therefore, the oxidation of Au(s) is unlikely to occur under given conditions. However, the resulting Au nanoplates initially show sharp vertexes and they become gradually rounded as a function time, indicating that the vertex atoms are more labile than other surface atoms to the chemical change of medium. The selective etching of Au triangular nanoplates indicates that dissimilar crystallographic planes react differently toward the change of chemical environments. Unlike the Au(111) terrace atoms (flat domain), which have a surface coordination number, CN, equal to 9, the vertex sites have surface atoms with low CN (<6), so that most of the $AuCl_4^-$ ions react with the lower-coordination (or higher-energy) sites rather than with terrace facets. It also implies that the standard redox potential of the sharp vetex sites is lower than 0.926 V, and therefore the oxidation of vertex ($Au_{vertex}(s) + 2Cl^- \rightarrow AuCl_2^- + 2e^-$) occurs as $AuCl_4^-$ ions become reduced. When the chemical condition of medium is changed to the mild reduction

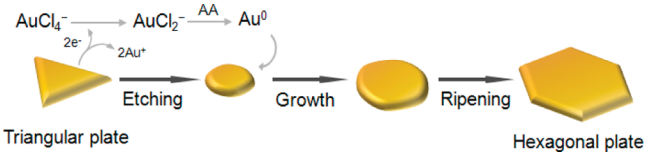

Figure 1. Procedure for the shape transformation from triangular to hexagonal nanoplates. AA is ascorbic acid.

Received: November 14, 2010
Revised: February 21, 2011
Published: March 29, 2011

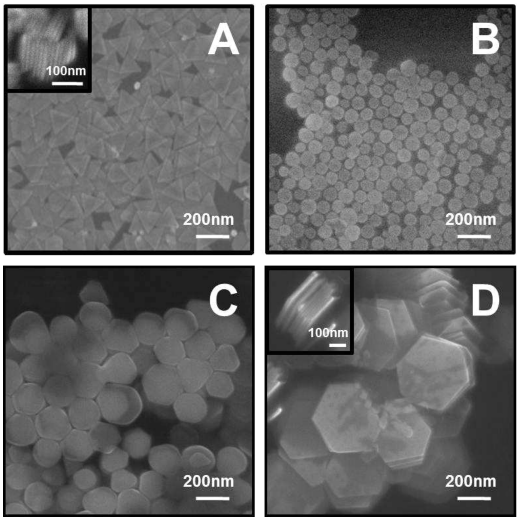

Figure 2. FESEM images for Au nanoplates corresponding to the cartoon shown in Figure 1. (A) Triangular nanoplates (edge L = 136 (±8) nm, thickness t = 8 (±1) nm), (B) nanodisks after tip etching (diameter d = 76 (±7) nm), (C) shape transformation to hexagonal nanoplates (edge L = 97 (±20) nm), (D) final shape of hexagonal nanoplates after shape transformation (edge L = 210 (±23) nm, thickness t = 19 (±2) nm). Left upper shows the side-view of Au nanoplates.

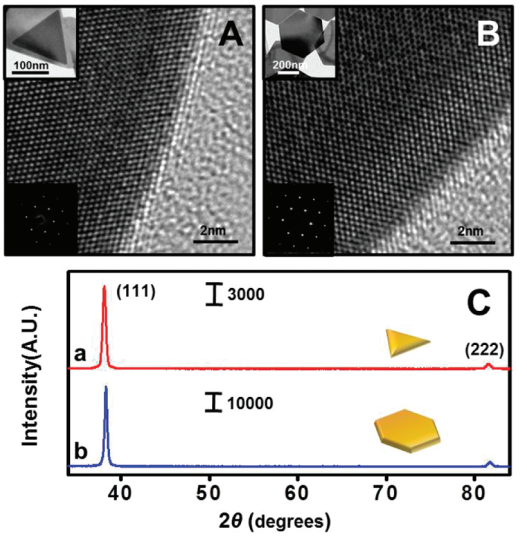

Figure 3. HRTEM images of (A) triangular nanoplate, (B) hexagonal nanoplate. Left upper and lower insets show the TEM image and diffraction pattern of the flat surface, respectively. (C) The X-ray diffraction pattern (XRD) of Au nanoplates: (a) triangular, (b) hexagonal nanoplates .

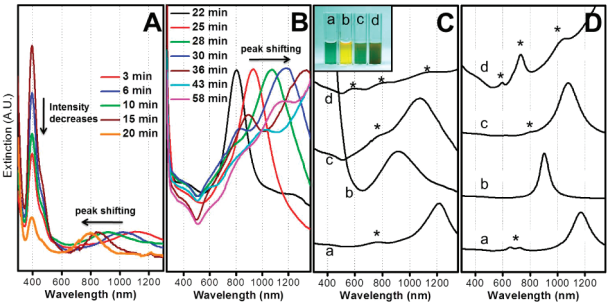

Figure 4. (A) Time-resolved UV−vis−NIR spectra of the etching process of triangular nanoplates after adding $AuCl_4^-$ to the solution. (B) Time-resolved UV−vis−NIR spectra of growth process of nanodisks after adding ascorbic acid to the nanodisk solution. (C) UV−vis−NIR spectra corresponding to nanoplates shown in Figure 1; (a) triangular Au nanoplates, (b) nanodisks, (c) small hexagonal nanoplates during the growth process, (d) large hexagonal nanoplates after the growth process. Insets in C show the photograph images when they are dispersed in water. (D) Calculated extinction spectra corresponding to panel C. Asterisk marks indicate the higher-order plasmon resonance band of each sample. Spectra in A and B are normalized.

environment by slowly adding ascorbic acid, $AuCl_2^-$ ions start to be reduced on the edge of nanodisks and the resulting shape of nanoparticles is hexagonal nanoplates. The observed shape transformation of nanodisks proceeds without any new nucleation events. The average size of the newly formed nanoplates depends on the amount of $AuCl_2^-$ ions present in the solution. The edge length can be tuned within the range from 100 to 350 nm and the thickness from 19 to 170 nm (see the Supporting Information).

Figure 3 shows HRTEM images and XRD patterns of Au nanoplates. Fringe spacing (0.24 nm) and diffracions patterns of triangular and hexagonal nanoplates indicate that {111} surface were exposed on the top surface. The results suggests that the crystal structures were retained during the selective etching of the triangular nanoplates and regrowth of nanodisks. Also, the XRD pattern of triangular nanoplates is identical with that of hexagonal nanolates.

The nanoplates shape transformation steps have been monitored with time-resolved UV−vis- NIR spectroscopy (Figure 4, in panel A and B). In the etching process (panel A), the spectra clearly reveal two distinct changes, the first of which is the peak shift at 1119 nm to shorter wavelength (at 800 nm after 20 min) as the tips of triangular nanoplates become rounded. This band is assigned to the in-plane dipole resonance associated with the Au nanoplates. Concurrently, the peak intensity at 395 nm, which is the feature of $AuCl_4^-$, becomes weak as a result of $AuCl_4^-$ reduction. The reduction of $AuCl_4^-$ occurs as a result of the presence of reducing agent (ascorbic acid) and the oxidation of Au_{vertex}(s) of triangular nanoplates. When a certain amount of ascorbic acid was added to the same solution, the reduction of $AuCl_2^-$ occurs on the edge of nanoplates and the resulting evolution profile of spectra is displayed in panel B. During the growth process (panel B), the peak position of the in-plane dipole resonance gradually red shifts as the particles transform into hexagonal nanoplates. The peak observed at 800 nm shifts to 1180 nm and additional band appears at $\lambda_{max} \approx 820$ nm after 30 min (blue line). The second band initially at ~750 nm red shifts as the growth process continues. This band is assigned to an in-plane quadrupole resonance of the Au hexagonal nanoplates, and appears in the NIR at 1140 nm in conjunction with additional bands that appear at 845 and 600 nm at the end of the growth process (purple line after 58 min). The peak shift reflects an increase in nanoplate edge length and the appearance of additional bands indicates the formation of hexagonal nanoplates. The assignment of these bands is based on discrete dipole approximation (DDA) calculations (see the Supporting Information for details about the method and model particles), which predict plasmon resonance bands that match experimental

dx.doi.org/10.1021/cm103273c |*Chem. Mater.* 2011, 23, 2011–2013

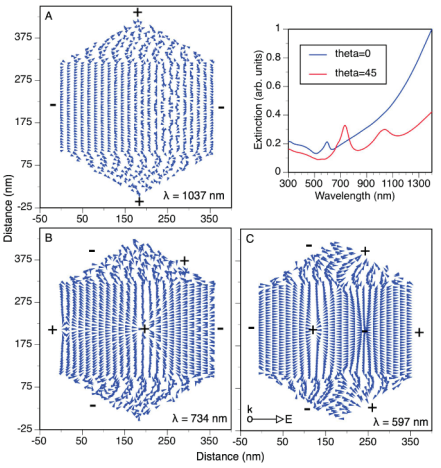

Figure 5. Polarization of a hexagonal nanoplate with a 210 nm edge length and 19 nm height. The plots show a surface plane of the particle, where 90% of the dipoles have been removed for viewing clarity. Panels A, B, and C correspond to three different multipoles (when $L = 2, 3, 4$). The particle orientation with respect to incident field is shown in panel C. The orientation for panels A and B corresponds to 45° rotation into the page about the axis perpendicular to both k and E depicted in Panel C. The inset shows the calculated extinction for these two orientations ($\theta = 45$ for panels A and B, and $\theta = 0$ for panel C).

observation. Experimental and theoretically calculated spectra corresponding to each different nanoplate described in Figure 1 are plotted in Figure 4C and D with asterisk marks on higher-order plasmon resonance bands, respectively. The resonance frequencies are in excellent agreement. There are some differences in the peak widths that result from inhomogeneous broadening in the experimental measurements and could also be attributed to the choice of dielectric constant used in the calculations. Spectrum *a* matches the previously reported result associated with triangular nanoplates, showing the in-plane quadrupole mode at 760 nm, reflecting the high quality of sample. There is an additional weak resonance predicted by theory at ~660 nm, which is unresolved experimentally, but is consistent with calculations performed previously on triangular prism nanoparticles.[13,17] When the tips of the triangular nanoplates are etched to form disks, DDA calculations show a blue shift of the dipole resonance in agreement with the experimental peak located at 920 nm. As the growth process proceeds, a dipole resonance of hexagonal nanoplates appears at 1080 nm in addition to a shoulder at 770 nm (quadrupole mode). The red shift results from the particles becoming larger and the sharper features of a hexagonal cross section compared to the smooth disks. Spatial regions near tips or edges obtain field-induced polarizations more readily than smooth surfaces (i.e., it is easier for the nanoparticle to polarize), which results in red shifts of the plasmon modes. This is consistent with the lightning rod effect noted in spheroidal particles, where large fields reside in regions of high curvature and the plasmon resonances shift to longer wavelengths. Significantly, a UV−vis−NIR spectrum of large, hexagonal nanoplates and a corresponding simulated spectrum from DDA calculations are in good agreement (spectrum *d* in panel C and D, respectively). For trace D, the dipole mode is beyond the investigated spectral window and a quadrupole mode is observed in both experiment and theory around 1100 nm, as are other higher-order modes appearing at approximately 800 and 580 nm. Figure 5 shows the polarization of a large hexagonal nanoplate (see the figure captions and the Supporting Information for details).

In conclusion, we present a simple synthetic method for hexagonal Au nanoplates in pure form. Selective etching of specific facets of nanoplates has led to the shape transformation. This contribution exemplifies the site-dependent reactivity of nanoparticles. As demonstrated in the field of catalysis, the site-dependent reactivity of nanoparticles can be used for selective etching and growth of specific facets by controlling experimental conditions. Also, the high quality of such materials allows one to identify the higher-order plasmon resonance bands including the dipole mode, which is important in terms of physical property characterization as well as their optical applications.

AUTHOR INFORMATION

Corresponding Author

*To whom correspondence should be addressed. (K.L.S.) e-mail: shuford@drexel.edu. (S.P.) e-mail: spark72@skku.edu.

ASSOCIATED CONTENT

Supporting Information. Experimental details Au hexagonal nanoplate synthesis, and DDA calculation. This material is available free of charge via the Internet at http://pubs.acs.org.

ACKNOWLEDGMENT

This work was supported by the National Research Foundation of Korea (World Class University (WCU): R31-2008-10029, Nano R&D program: 2010-0019149, 2010-0015457, and Priority Research Centers Program: NRF-20100029699). K.L.S. thanks Drexel University for start-up funding.

REFERENCES

(1) Barnes, W. L.; Dereux, A.; Ebbesen, T. W. *Nature* **2003**, *424*, 824.
(2) Bohren, C. F.; Huffman, D. R. *Absorption and Scattering of Light by Small Particles*; John Wiley: New York, 1983.
(3) Henglein, A. *Chem. Rev.* **1989**, *89*, 1861.
(4) Burda, C.; Chen, X.; Narayanan, R.; El-Sayed, M. A. *Chem. Rev.* **2005**, *105*, 1025.
(5) Wang, J.; Wang, Z. *Mater. Lett.* **2007**, *61*, 4149.
(6) Lofton, C.; Sigmund, W. *Adv. Funct. Mater.* **2005**, *15*, 1197.
(7) Brown, K. R.; Walter, D. G.; Natan, M. J. *Chem. Mater.* **2000**, *12*, 306.
(8) Chen, J.; McLellan, J. M.; Siekkinen, A.; Xiong, Y.; Li, Z.-Y.; Xia, Y. *J. Am. Chem. Soc.* **2006**, *128*, 14776.
(9) Tao, A.; Sinermsuksakul, P.; Yang, P. *Angew. Chem., Int. Ed.* **2006**, *118*, 4713.
(10) Kim, S.; Shuford, K. L.; Bok, H.-M.; Kim, S, K.; Park, S. *Nano Lett.* **2008**, *8*, 800.
(11) Jana, N. R.; Gearheart, L.; Murphy, C. J. *J. Phys. Chem. B* **2001**, *105*, 4065.
(12) Kim, S.; Kim, S. K.; Park, S. *J. Am. Chem. Soc.* **2009**, *131*, 8380.
(13) Millstone, J. E.; Park, S.; Shuford, K. L.; Qin, L.; Schatz, G. C.; Mirkin, C. A. *J. Am. Chem. Soc.* **2005**, *127*, 5312.
(14) Millstone, J. E.; Wei, W.; Jones, M. R.; Yoo, H.; Mirkin, C. A. *Nano Lett.* **2008**, *8*, 2526.
(15) Millstone, J. E; Hurst, S. J.; Metraux, G. S.; Cutler, J. I.; Mirkin, C. A. *Small* **2009**, *5*, 646.
(16) Harris, D. C. *Quantitative Chemical Analysis*; Freeman W. H. and Company: New York, 2003.
(17) Shuford, K. L.; Ratner, M. A.; Schatz, G. C. *J. Chem. Phys.* **2005**, *123*, 114713.